Volume 17, Issue 2, 172514 (1-14)

Iranian Journal of Earth Science (IJES)

https://doi.org/10.57647/j.ijes.2025.1702.14

Migmatite marvels: Unveiling the mysteries of high-grade metamorphism in Qandol, Bulfat mountain, Kurdistan region of Iraq

Kurda Latif Abdulla[1], Yousif Osman Mohammad[1,*], Hossein Azizi[2]

[1]*Department of Earth Science and Petroleum, College of Science, University of Sulaimani, Sulaymaniyah, Iraq.*
[2]*Department of Mining Engineering, Faculty of Engineering, University of Kurdistan, Sanandaj, Iran.*

[*]**Corresponding author:** yousif.mohammd@univsul.edu.iq

Original Research

Received:
11 March 2024
Revised:
12 June 2024
Accepted:
15 September 2024
Published online:
10 April 2025

Abstract:

In this paper, we introduce the migmatitic rocks in the Qandol area as a part of the Bulfat Igneous Complex (BIC) complex in the Zagros Suture Zone, northeast Iraq for the first time. The main protolith is mafic rocks which are preserved in some areas. Meanwhile, the partially melted parts (leucosomes) have a trondhjemite composition, with plagioclase being the dominant mineral phase. Geochemical analysis reveals that the leucosomes portion exhibits higher concentrations of Na_2O and CaO, accompanied by lower levels of K_2O, indicating a stronger association with calc-alkaline features. Meanwhile, the melanosome demonstrates a tholeiitic nature, attributed to its elevated content of compatible elements like Mg and Fe within the residual materials such as amphibole and pyroxene. The thermobarometry assessment indicates that the leucosome parts were crystallized at a temperature of $670-700\ ^{O}C$ and a pressure near 0.1 GPa. Furthermore, phase equilibrium modeling using the GeoPS software indicates initial melting has occurred at $790\ ^{O}C - 920\ ^{O}C$ and $0.1-0.4$ GPa. The estimating of the P-T of the present migmatite infers that the metamorphism has occurred at high temperature and low pressure either in the root of the mature arc or in a shear zone as a result of hot oceanic subduction beneath the Sanandaj-Sirjan Zone (SaSZ) in the late Cretaceous or younger. The presence of the high-T migmatite in the Zagros Sutures Zone without a clear relation to the sole metamorphism in the base of ophiolite members in the Qandol area would be much more useful to understand the tectono-magmatic processes in the pre- to syn-collision regime during the closer of the Neotethys ocean.

Keywords: Migmatite; Gabbro; Partial melting; TTG; Orogenic belts; Neotethys subduction

1. Introduction

Migmatite can originate through the metamorphism of either meta- pelitic or meta-mafic rocks at high temperatures during regional or contact metamorphic events. Moreover, it has been recognized as a transitional entity between metamorphic and igneous rocks (Brown et al., 1995; Sawyer, 2010). On a megascopic scale, migmatite exhibits heterogeneity characterized by bimodal or trimodal variations in its petrographic domains. The leucosome, which represents the partially melted portion, typically consists of light-colored minerals like quartz and feldspars or feldspathic compositions. It is enriched in non-refractory elements such as silica, sodium, potassium, light rare earth elements (LREE), and incompatible elements. Meanwhile, the darker-colored melanosome contains higher concentrations of refractory elements including aluminum, iron, calcium, heavy rare earth elements (HREE), and compatible elements.

Additionally, ferromagnesian minerals like biotite, garnet, cordierite, orthopyroxene, and hornblende are prevalent in the solid residue parts (Ashworth and McLellan, 1985; Sawyer and Brown, 2008, 2008; Maxeiner et al., 2017). Field criteria suggest three types of leucosomes, based on the melt-residuum relationship: (1) in situ (melt in close association with residuum), (2) in-sources (migrated a short distance from residuum), and (3) injected (moved a long distance from the melting site) (Sawyer and Brown, 2008; Pawley et al., 2013).

Since migmatite originates from a parent rock of bimodal origin, the geochemical characteristics and mineral compositions within different parts of the migmatite can serve as a valuable record of the source rock's nature. These

signatures also provide insights into the processes driving migmatite formation across various tectonic and metamorphic settings within high-temperature orogenic belts.

The Bulfat Igneous Complex (BIC), cover an area of about $\sim$ 100 km^2 is juxtaposed with parts of the Sandaj Sirjan Zone (SaSZ) of upper Iranian plate affinity, located on the lower Arabian. The emplacement of the entire BIC occurred due to ongoing, gradual subduction-related thrusting, resulting from the convergence and eventual collision of the upper (Iranian) and lower (Arabain) plates in the Kurdistan region of Iraq (Fig. 1). This study marks a pioneering endeavor in the identification of the mafic migmatite within the Iraqi Zagros orogenic belts, offering essential insights into the underlying dynamics of the collision processes in this region. This research particularly focuses on petrology, and geochemistry to fulfill the migmatite zone gap with the collision zone, by providing detailed field and petrographic observations, linked with available published geochronological data on various migmatite types and related rocks in the Bulfat igneous metamorphic complex.

2. Geology setting

Northern Iraq is tectonically categorized into two primary tectonic regions, namely the Western Zagros Fold Thrust Belt and the Sanadanj-Sirjan Zone (SaSZ), the later often referred to as the Shlair Zone in Iraq (**Fouad2015**). The Western Zagros Fold Thrust Belt can be further subdivided into four parallel tectonic zones from the northeast to the southwest, namely, the Zagros Suture Zone, Imbricated Zone, High Folded Zone, and Low Folded Zone (Fig. 1).

The Zagros Suture Zone, as described by **Fouad2015<empty citation>**, can be divided into two minor significant subzones: the Qulqula-Khwakurk subzone and the Penjween-Walash subzone (Fig. 1). Within the Zagros Suture Zone, there are four well-recognized magmatic and metamorphic zones, which are Penjween, Mawat, Bulfat, and Hassanbag complexes from southwest to northeast. These complexes, are believed to be representative of fossil fragments from the Late Cretaceous to Paleocene ophiolite, originating from the oceanic crust and upper mantle of the Neotethys ocean Buda (1993), Jassim and Goff (2006), Aswad et al. (2011), Mohammad et al. (2014), and Ali (2017).

Within the frame of the regional tectonic anatomy of the Zagros orogenic belt Gurbuz and Saein (2019), the Zagros orogenic belt in the Kurdistan region of Iraq encompasses three parallel NW-SE-trending tectonic units. These are (1) the Sanandaj–Sirjan Zone, (2) the Imbricate Zone (including Zagros Suture Zone), and (3) the Zagros Fold and Thrust Belt (Mohammad et al., 2014; Le Garzic et al., 2019). The 40 km wide Sanandaj–Sirjan Zone (SaSZ) in the Kurdistan region of Iraq occupies an area

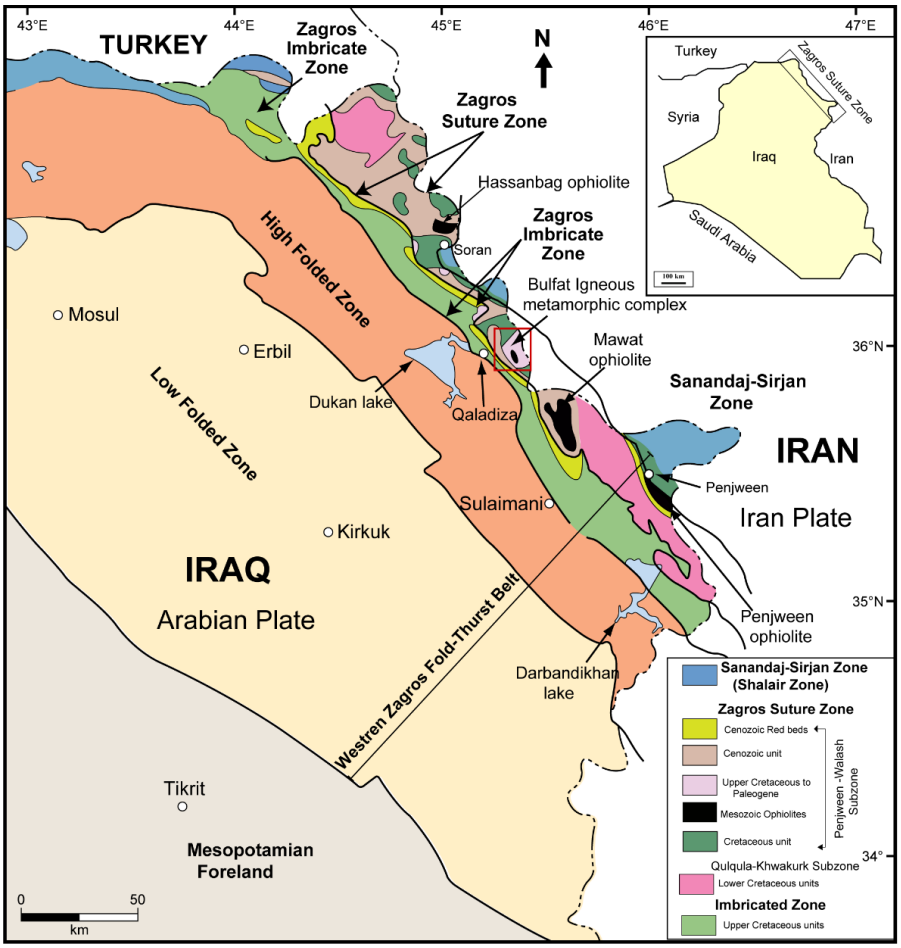

Figure 1. Regional tectonic map of the northeastern Iraq showing the Zagros suture zone, in addition to distribution of Mesozoic Neo-Tethyan ophiolites (after (**Fouad2015**; Mohammad et al., 2016).

of about $700 - 900$ km^2. It representing the complete narrow V-shaped salient in the Penjween area in the south west in addition to the Qandil mountain in the Qaladiza area, with some part of Hasarost mountain near Soran city in the northeast. The BIC is located within the ZSZ of Iraq, at the boundaries between the Arabian and Iranian plates. Previously, this complex was subdivided into an upper allochthon represented by BIC, and a lower allochthon represented by the Walash-Naopurdan volcanic sedimentary sequence separated by the main thrust fault (Aswad et al., 2011; Aziz et al., 2011). The BIC covers an area of about 100 km^2 and is located 65 kilometers north of Sulaimaniya city and 30 kilometers northeast of Qala-Diza town (Jassim and Goff, 2006; Aswad et al., 2011; Ali, 2017; Nutman et al., 2022). The complex consists of huge semi-layered igneous intrusions intruded into or caped by the various types of metasedimentary rock units of the Albian–Cenomanian Gimo–Qandil sequence in the Qaladiza area.

From the bottom to the top, the igneous rocks consist of a mantle peridotite followed by strongly differentiated gabbro-metagabbro, then to the S, I-type granite and nepheline syenite at the top. The whole BIC has undergone a series of complex metamorphic overlapping stages, regional, dynamic, and hydrothermal metamorphism. As a result, distinguishing the individual stages of metamorphism is a challenging endeavor. The metagabbro units are the most dominant units with nest nature intrusion, consisting of two mafic pulses (Ali, 2017). The whole igneous intrusion is capped by meta-carbonate and metapelite with clear contact metamorphism along the border of Qandil unit, with evident skarn mineralization. The grade of the metamorphic increases toward the igneous body, with a maximum grade of sanidine facies. Occasionally, assimilation of the country rocks is observed within the mafic unit.

The southern and northern region of the BIC is predominantly composed of metagabbroic rocks, as shown in Fig. 2. Meanwhile, the central part of the complex hosts olivine gabbro with low grade metamorphism. The imprint of

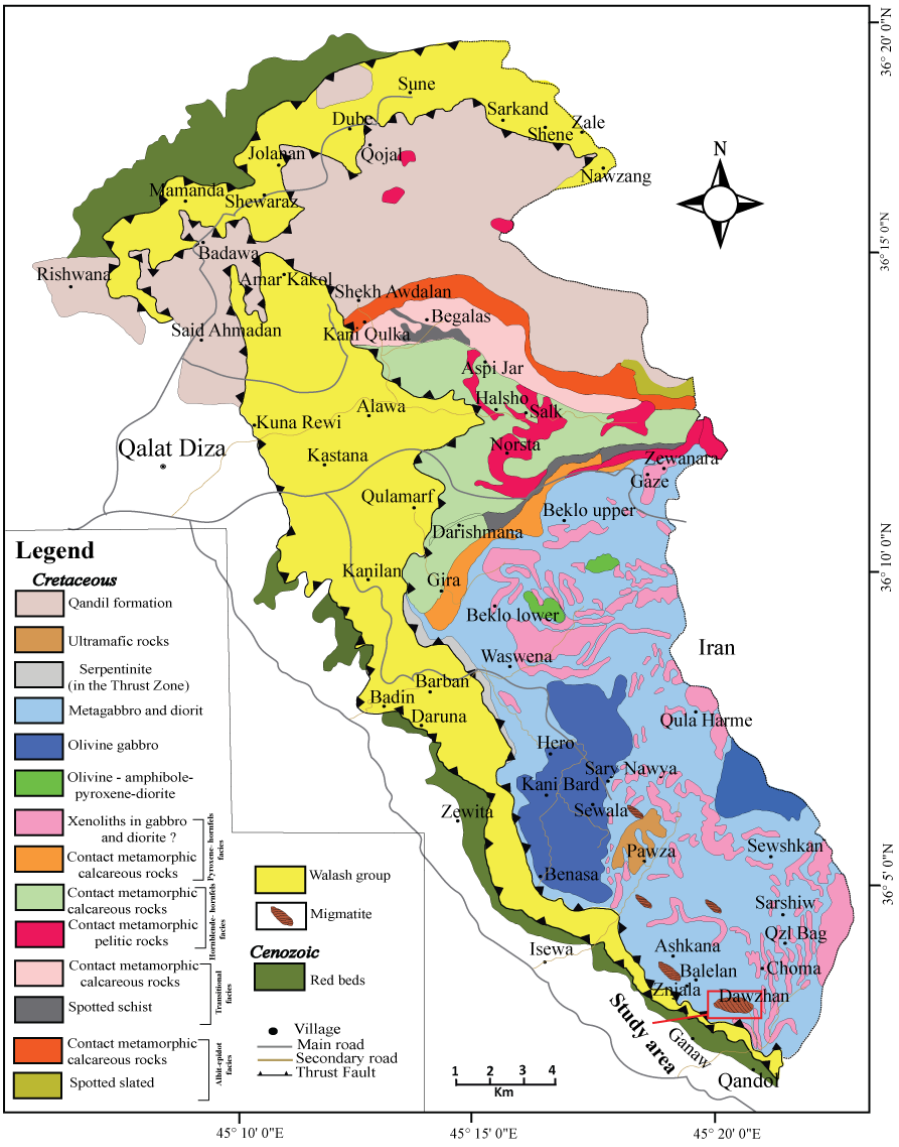

Figure 2. Regional Geological map of the Bulfat Igneous Complex, Qaladiza, NE Iraq (modified after (Buda, 1993).

regional metamorphism is evident through compositional layering and ductile deformation in metagabbro. However, the clear contact between migmatite and metagabbro is obscured due to extensive deformation and internal deformation within the BIC, compounded by soil cover in the area. Field observations shows gradual changes from metagabbro to migmatite in the Qandol area.

The Bulfat Igneous complex has been dated to approximately 34.78 million years ago using the ^{39}Ar-^{40}Ar dating method Karo et al. (2018), while Ali (2017) employed U-Pb dating of a single zircon grain and suggested an age of roughly 39.0 ± 0.5 million years for the same igneous complex. Nutman et al. (2022) suggested that the granite within the BIC, estimated to be around 48 million years old, resulted from the partial melting of previously recycled mafic crust. Additionally, Elias et al. (2022) provided evidence indicating an intrusion within the Bulfat Igneous Complex predating 50 million years. Mohammad et al. (2023) presented the detailed geochemical and petrological studies of various rock types (felsic to mafic) from Bulfat Igneous Complex. Based on U-Pb dating, major and trace element compositions and Sr-Nd isotope compositions, Mohammad et al. (2023) identified that Bulfat mafic rocks are likely originated from a well-developed are tectonic regime in the Neotethys ocean at $70 - 64$ Ma ago.

3. Field observations

3.1 Mafic rocks

The gabbroic rocks, which is the most significant exposure of mafic rocks in the central part of study area (Fig. 2), are found in the BIC together with several forms of tonalitic migmatites near the south west outer margin of the body. Meanwhile, the northern eastern boundary is within meta carbonate of the Qandil unit at the top and the Walash volcanic group at the bottom. Such that both the BIC and Qandil unit thrusted over the Walash volcanic group. A slice of metaperidotite is sandwiched between meta olivine gabbro and migmatite in the southern part of BIC.

3.2 Metamorphic rocks

The mafic rocks are the dominant components of the intrusive bodies within the BIC. The most significant exposure of mafic rocks in the study area is metagabbro (Figs. 3 a and b). The rock is intersected by numerous I and S-type feldspathic sills and dykes that cut deformed metagabbro (Fig. 3 c). Generally, within the study area, dynamic deformation has been intensely observed in the field.

In addition to the mylonitic fabric found in most rock types of the BIC, variable strain rates in hard and ductile zones, such as the mylonitic foliation, augen structure, and isoclinal folds, were generated (Figs. 3 d and e). The sedimentary rocks intermixed with fine-grained metagabbro and carbonate rocks in the contact zone show the presence of an intrusive host of sedimentary rocks in the BIC (Fig. 3 f).

Petrographical observations in addition to field observations reveal that the textures and chemical properties of protolith rocks did not change much during the collisional-related metamorphic event. Close to the outer margin, the country rocks represented by mafic and carbonate rocks, underwent intense thermal metamorphism as a result of a gabbro intrusive body that created a 2.5 km wide metamorphic aureole (Elias et al., 2022). The development of migmatites and hornfels is a characteristic of contact aureole for mafic and meta carbonate rocks respectively. The migmatites are well developed on the southern side of the BIC, near the ultramafic unit on the Iran border, because of their varied lithologies and partial melting conditions, the examined migmatites display a variety of structural patterns

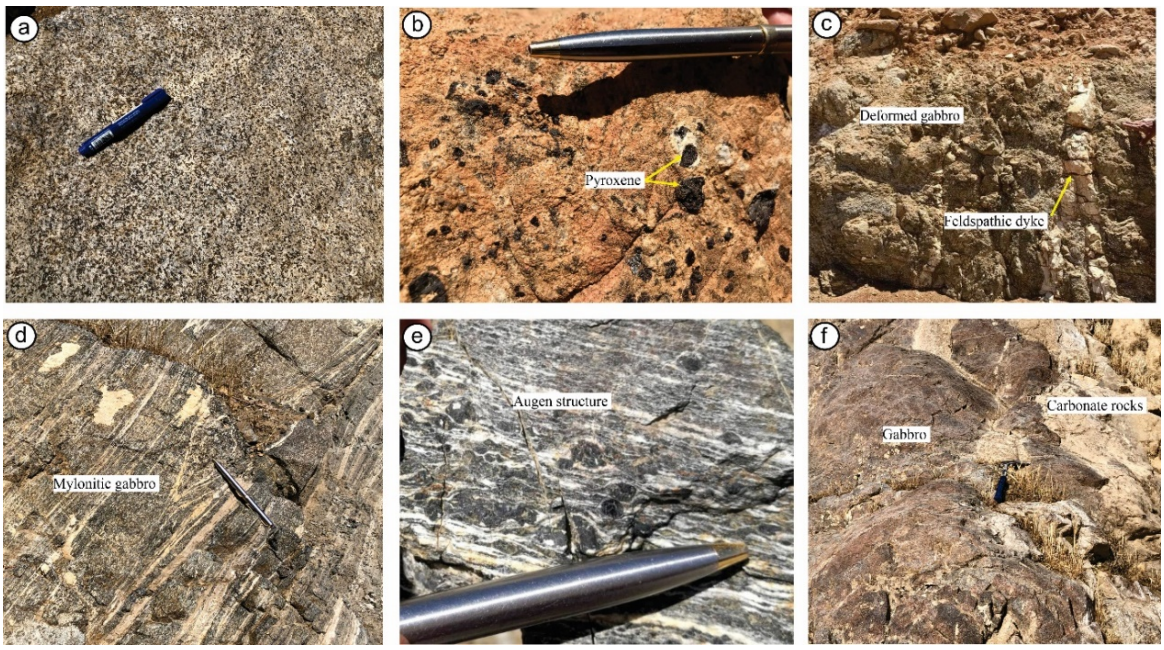

Figure 3. Field observation of BIC showing: (a) Fine-grained gabbro (b) Gabbro with large pyroxene crystal. (c) deformed metagabbro cut by vertical feldspathic dykes. (d, e) Dynamic deformation results in mylonitic texture, augen structure. augen structure (mylonitic texture). (f) Contact between massive gabbro and meta-limestone (marble) of Qandil unit.

in outcrop. On the outcrop scale, the leucocratic migmatite displays both in-source leucosomes and in situ leucosomes (Fig. 4).

Notably, the leucosome volumes are relatively lower compared to the melanosomes. The range of migmatites observed in the research area spans from metatexite to diatexite. Metatexite is characterized by stromatic, patch, and net structures, while diatexite migmatite presents in nebulite and fold structures. The prevalence of stromatic migmatites points to extensive large-scale partial melting and migmatization within the BIC (Figs. 4 a-f). The migmatite formations also exhibit common deformation features, including extensional shear bands and boudin necks filled with regional melt segregations (Fig. 4 f).

The observed stromatic structures serve as indicators of strain resulting from partial melting (**Sawyer1998**; Sawyer and Brown, 2008). A common sign of melt migration towards areas of lower strain is the presence of leucosome-filled boudin necks, a phenomenon that is frequently observed within stromatic migmatites (Weinberg and Mark, 2008; Pawley et al., 2013). Significant deformation within the region has led to the creation of fold-structured leucosomes, which in turn can facilitate the migration of partial melts, as evident in (Figs. 4 g and h). Conversely, in instances where the proportion of melt is slightly higher, the neosome adopts an in-situ patch structure (Fig. 4 i). This patch structure is notable for its significantly coarser grain size compared to the surrounding paleosome. In addition to the aforementioned migmatite forms, nebulite diatexites represent another distinct morphology found in the area. It's worth noting that while nebulite diatexites are present, they are less common than the other types of migmatites discussed earlier.

4. Petrography

The undeformed gabbroic rocks, which are the primary protolith of the migmatites have a medium-to coarse-grained, hypidiomorphic granular, cumulate texture (Fig. 5). The dominant mineral assemblage within the protolith consists of euhedral to subhedral plagioclase ($60-70$ vol%), olivine ($10-15$ vol%), and anhedral clinopyroxene ($10-20$ vol%), and hornblende (Figs. 5 a-c). Accessory minerals such as opaque mineral, zircon, and occasionally sphene are also present. Frequently, hornblende exhibits secondary minerals in the gabbroic rocks and makes a coronitic reaction rim with pyroxene (Fig. 5 c) and olivine, which was formed during the retrograde stage of metamorphism.

The petrographic characteristics of the different migmatite components can be described as follows: (i) The melanosome exhibits a medium-to-coarse-grained texture and displays a variable foliation pattern. It mainly comprises recrystallized hornblende ($50-60$ vol%) and anhedral metamorphic plagioclase ($40-50$ vol%). In addition to these minerals, accessory minerals such as opaque

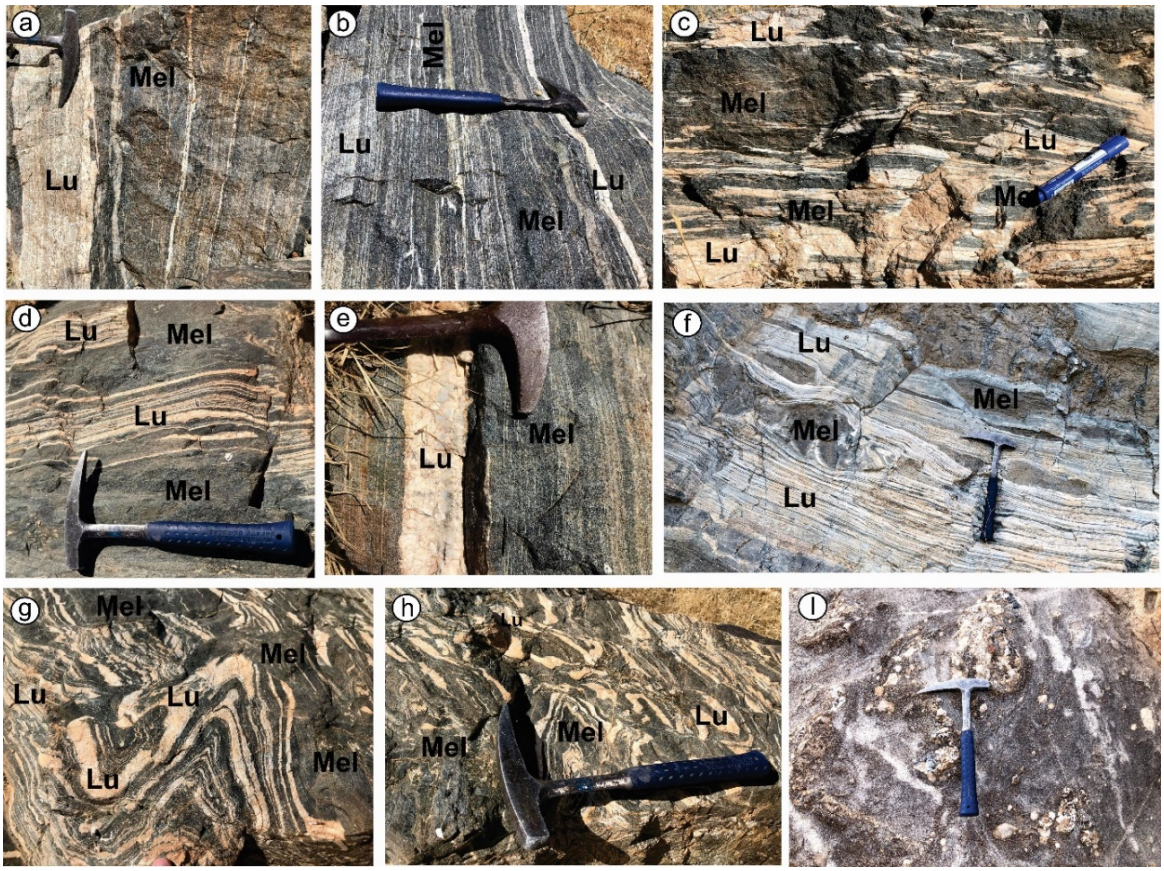

Figure 4. Field photographs of Qandol migmatites. (a-f) in source stromatic migmatite. (a-e) Parallel direction of leucosome, in a stromatic metatexite. (f) Layer-parallel leucosomes and melanosomes with local melt segregation into boudin necks and extensional shear bands are characteristics of stromatic migmatites. (g, h) Fold stromatic leucosome structure, an indication of in-source migmatite (i) Patches of metatexite texture represent in-situ partial melting. *Abbreviations; Mel: melanosome; Lu: leucosomes.*

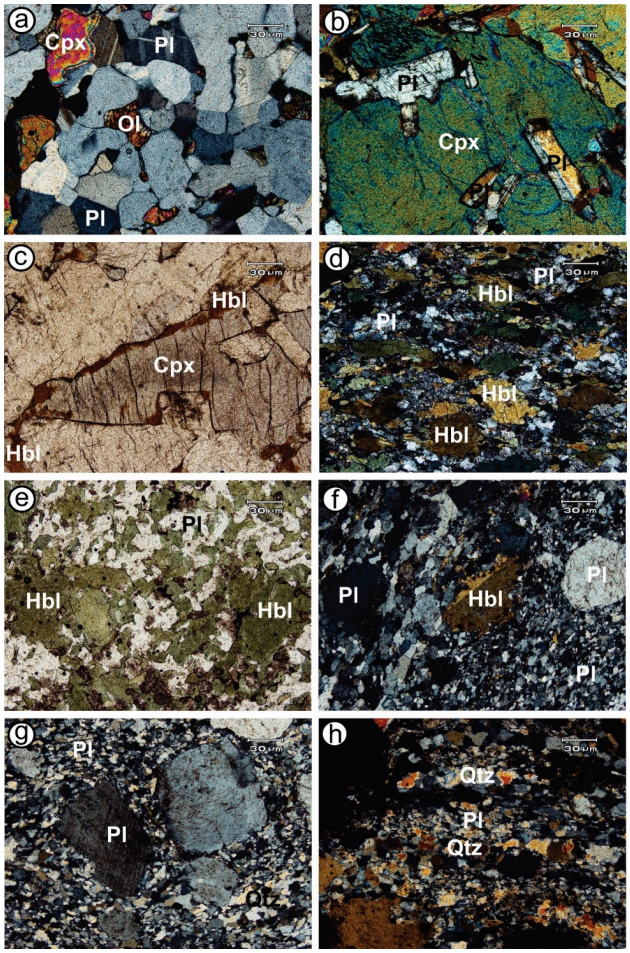

Figure 5. Photomicrographs of the Qandol migmatites. (a) Coarse-grained gabbro with hypidiomorphic, granular texture. (b) lath plagioclase is enclosed by pyroxene as a poikilitic texture. (c) Pyroxene is bounded by coronitic hornblende in the gabbro. (d, e, f) melanosome display foliation texture. (g) leucosome characterized by mylonitic texture in granitic rocks. (h) quartz ribbon structure within leucosome migmatite. Abbreviations: *Hbl = hornblende, Pl = plagioclase, CPx = clinopyroxene, Qtz = quartz, Ol = olivine.* (Mineral abbreviations after (Whitney and Evans, 2010).

minerals, sphene, apatite, and calcite are present (Figs. 5 d and e). (ii) The leucosome samples show a fine-to-coarse grain size with an inequigranular to mylonitic texture. The primary mineral assemblage is dominated by anhedral plagioclase (60 – 70 vol%), quartz (constituting 20 – 30 vol%), and k-feldspar (10 – 15 vol). Minor amounts of amphibole (2 vol%) are also present. Additionally, accessory minerals like biotite, opaque minerals, apatite, monazite, and zircon are observed (Figs. 5 f-h). The compositions of the leucosomes span from tonalite to trondhjemite, which is determined based on the measured proportions of these minerals.

5. Analytical methods

Fifty thin sections were precisely crafted from the mafic migmatite, encompassing both leucosome and melanosome sections, as well as the source protolith. These thin sections were then examined using transmitted light microscopy to enable a detailed petrographic characterization. Out of these sections, a subset of ten samples, chosen to be representative, underwent whole-rock analyses. These analyses encompassed the determination of major, trace, and rare earth elements (REEs). The techniques employed for these analyses involved X-ray fluorescence and inductively coupled plasma mass spectrometry (ICP-MS). To facilitate these analyses, the samples were initially decomposed using a $LiBO_2$ flux, followed by dissolution with HNO_3. These procedures were conducted at the ALS Laboratory Group located in Spain, and the analytical package used was ME-MS 81d along with ME-4ACD81 for comprehensive whole rock analysis. The outcomes of these geochemical analyses are detailed in (Table. 1). Thermodynamic modeling was conducted using the Geo-Pseudo 3 Section software (Xiang and Connolly, 2022).

6. Geochemistry (sources, melanosome and leucosome)

6.1 Source portion

Major, trace, and rare earth element compositions of the origin gabbro, leucosomes, and melanosomes of migmatites are listed in (Table. 1). Gabbro contains SiO_2 in a range of 48.3 to 51.4 wt.%, Al_2O_3 (16.75 – 20.2 wt.%), Fe_2O_3 (4.94 – 10.7 wt.%), CaO (9.68 – 11.35 wt.%), MgO (5.67 – 9.36 wt.%), and Na_2O (2.73 – 4.26 wt.%). Gabbro is characterized by low K_2O (0.1 – 0.22 wt.%) and TiO_2 (0.33 – 2.61 wt.%) contents. On the total alkali versus silica (TAS) classification diagram Cox et al. (1979), the samples were plotted in the gabbroic field (Fig. 6 a), while in the AFM diagram Irvine and Baragar (1971), they were mostly plotted in the border of the tholeiitic and calc-alkaline series (Fig. 6 b).

The trace element normalized patterns in comparison to the primitive mantle Sun and McDonough (1989) display positive anomalies for Ba and Sr and negative anomalies for Rb, Th, Nb, and Zr for the source gabbroic samples (Fig. 7 a) and also rare earth element (REE) patterns Sun and McDonough (1989) which has a flat pattern (Fig. 7 b) with a positive Eu anomaly ($Eu/Eu^* = 1.4 – 1.8$). The total REE content is (14 – 44 ppm), and the gabbro has a less fractionation REE pattern [(La/Yb) N = 1.3 – 2.4]. The presence of a positive Eu anomaly may indicate the high contents of plagioclase grains in the gabbroic rocks, which have been considered protoliths of migmatites in this area.

6.2 leucosome portion

The leucosome portion contains high SiO_2 ranges varying from 74.2 to 76.1 wt.%, Al_2O_3 (14.4 – 14.6 wt.%), and Fe_2O_3 (1.56 – 2.1 wt.%), high Na_2O (5.2 – 5.56 wt.%), and CaO (2.4 – 3.3 wt.%), with low K_2O values (0.27 – 0.38 wt.%). Leucosome portions are chemically plotted in the granite field in the TAS diagram (Fig. 7 a) (Cox et al., 1979). The leucosome portions fall under the calc-alkaline series, as shown on the AFM diagram Irvine and Baragar (1971) and in the trondhjemite fields (Fig. 6 c), based on the normative values in the Ab-An-Or diagram (O'Conner, 1965). In comparison to, primitive mantle values Sun and McDonough (1989), strong Th and Pb positive anomalies and negative Rb, P, and Ti anomalies appear in the leucosome fraction (Fig. 7 a). In addition, a negative slope for the LREE to HREE (Fig. 7 b) with higher ratios of (La/Yb) n=

Table 1. Major, trace, and rare earth element concentrations of the Qandol migmatites (Mohammad et al., 2023).

	Source portion (gabbro)				Leucosome portion			Melanosome portion		
Sample	**QHK-13**	**QHK-29**	**QHK-38**	**QBA-20**	**QBA-4**	**QBA-8**	**QBA-9**	**QHK-8**	**QHK-15**	**QHK-21**
Major oxides (wt.%)										
SiO_2	51.4	48.3	49.8	50.5	74.2	76.1	74.7	40.4	42.1	41.8
TiO_2	0.75	0.73	0.33	2.61	0.23	0.08	0.13	1.62	1.56	2.41
Al_2O_3	17.55	18.2	20.2	16.75	14.6	14.45	14.4	14.35	9.84	7.53
Fe_2O_3	7	9.75	4.94	10.7	2.09	1.56	1.91	13.15	11.2	10.75
MnO	0.12	0.15	0.08	0.19	0.02	0.01	0.02	0.16	0.19	0.17
MgO	8.26	9.36	8.32	5.67	0.68	0.28	0.25	13.05	6.06	8.46
CaO	10.2	11.35	10.9	9.68	3.25	2.43	2.95	11.9	21.5	23.3
Na_2O	4.26	2.73	3.52	4.25	5.46	5.56	5.2	2.28	2.6	1.46
K_2O	0.13	0.09	0.1	0.22	0.29	0.38	0.27	0.47	0.29	0.24
P_2O_5	0.05	0.01	0.02	0.27	0.05	0.02	0.04	0.31	1.33	2.13
LOI	0.5	-0.03	0.97	0	0.67	0.76	0.51	1.13	1.89	1.39
Total	100.22	100.64	99.18	100.84	101.54	101.63	100.38	98.82	98.56	99.64
Trace elements (ppm)										
Ba	45.8	27.4	101.5	34	62.3	121	88.7	55.8	33.9	43.2
Cr	380	490	90	310	30	<10	<10	230	90	30
Cs	0.04	0.06	0.12	0.28	0.11	0.11	0.08	0.02	1.73	0.64
Ga	14.6	12	15.5	11.5	12.4	11.5	12.3	20.3	14.5	13.7
Hf	0.5	0.5	0.7	1.1	0.8	1.2	4.4	3.2	4.4	6.7
Nb	0.5	0.7	4	0.7	4.1	1.4	2.1	2.2	5.2	8.2
Rb	1.3	1.2	2.2	1.5	4.7	4.9	3.7	0.8	6.4	7.2
Sn	1	1	<1	1	1	1	1	1	4	4
Sr	344	337	275	281	429	395	504	279	151	229
Ta	<0.1	<0.1	0.3	<0.1	0.2	<0.1	0.1	<0.1	0.1	0.3
Th	0.13	0.17	0.24	0.14	3.47	2.36	12.3	0.28	2.54	2.4
U	<0.05	<0.05	<0.05	0.06	0.21	0.22	0.44	<0.05	0.96	0.66
V	341	74	380	144	17	<5	9	491	198	236
W	<1	<1	<1	<1	<1	<1	<1	<1	1	<1
Y	7.5	6.4	16.6	11.5	2.9	1.2	3.4	24.1	36.1	68.1
Zr	14	20	25	36	28	41	173	81	209	257
Ag	<0.5	<0.5	<0.5	<0.5	<0.5	<0.5	<0.5	<0.5	<0.5	<0.5
As	<5	<5	<5	<5	<5	<5	<5	<5	<5	<5
Cd	0.7	<0.5	1	0.5	<0.5	<0.5	<0.5	0.9	1	0.9
Co	47	36	35	36	4	2	2	63	33	39
Cu	75	107	47	36	6	98	21	121	39	37
Li	10	10	10	10	<10	<10	<10	10	20	10
Mo	<1	<1	1	1	1	<1	<1	<1	3	1
Ni	138	203	30	135	5	4	6	104	46	28
Pb	<2	<2	2	<2	<2	31	16	3	5	<2
Sc	26	19	40	26	2	<1	<1	65	29	24
Tl	<10	<10	<10	<10	<10	<10	<10	<10	<10	<10
Zn	67	29	78	41	27	15	18	96	95	83
Rare earth elements (ppm)										
La	1.8	1.4	4.4	2	10.4	6.2	46.3	13.3	22.3	30.3

Continue of Table 1.

Ce	4	3.5	11.3	5.3	17.2	10.4	79.7	43.2	47.2	74.9
Pr	0.59	0.57	1.79	0.9	1.81	1.17	8.4	7.27	5.71	10.25
Nd	3.1	2.9	9.5	4.9	6.4	3.9	28	41.1	27.7	52.2
Sm	1.04	0.93	2.98	1.63	1.01	0.65	3.34	9.16	5.89	11.45
Eu	0.68	0.64	1.68	0.88	0.38	0.35	0.8	3.02	1.64	2.87
Gd	1.6	1.27	3.9	2.22	0.78	0.41	1.74	7.86	7.18	13.5
Tb	0.2	0.16	0.53	0.32	0.07	0.01	0.13	0.94	1	2.15
Dy	1.54	1.26	3.4	2.4	0.51	0.26	0.75	5.25	6.67	12.65
Ho	0.27	0.21	0.63	0.42	0.06	0.01	0.11	1.02	1.33	2.62
Er	0.91	0.68	1.73	1.28	0.29	0.13	0.36	2.6	3.5	6.87
Tm	0.13	0.1	0.23	0.19	0.04	0.02	0.06	0.32	0.53	0.89
Yb	0.71	0.59	1.33	1.14	0.25	0.16	0.46	1.9	3.07	5.33
Lu	0.11	0.09	0.22	0.16	0.04	0.03	0.09	0.26	0.59	0.88
∑REE	16.68	14.3	43.62	23.74	39.24	23.7	170.24	137.2	134.31	226.86
Eu/Eu*	1.61	1.80	1.51	1.42	1.31	2.08	1.02	1.09	0.77	0.71
(La/Yb)N	1.82	1.70	2.37	1.26	29.85	27.81	72.23	5.02	5.21	4.08
TZr (C^o)					646.2	680.4	791.4			
Latitude	36.13739^{O}	36.15375^{O}	36.11136^{O}	36.06608^{O}	36.05186^{O}	36.05244^{O}	36.05244^{O}	36.05244^{O}	36.05244^{O}	36.05283^{O}
Longitude	45.27358^{O}	45.28789^{O}	45.27492^{O}	45.31683^{O}	45.34081^{O}	45.34111^{O}	45.34111^{O}	45.^{O}	45.34111^{O}	45.34808^{O}

$28-72$ and a strong positive Eu anomaly (Eu/Eu* $=1-2$).

6.3 Melanosomes portions

Melanosome portions have low SiO_2 in the range ($40.4-41.8$ wt. %), Al_2O_3 ($7.53-14.35$ wt. %), and higher Fe_2O_3 range from ($10.75-13.15$ wt.%), CaO ($11.9-23.3$ wt%), MgO ($6.1-13.1$ wt%) TiO_2 ($1.56-2.41$ wt%) and P_2O_5 ($0.31-2.13$ wt%). with lower content of Na_2O ($1.46-2.6$ wt.%), K_2O ($0.24-0.47$ wt%). This portion of chemical plots in the gabbroic field (Fig. 6 a) is due to the low content of alkali elements in the TAS diagram (Cox et al., 1979). On the AFM diagram Irvine and Baragar (1971), the samples are affinity to the tholeiitic series (Fig. 6 b) due to their high Fe_2O_3 content. Compared to the primitive normalized patterns (Sun and McDonough, 1989). Melanosome parts show negative anomalies of Ba, Sr, Zr, and Ti, with slight Pb positive anomalies (Fig. 7 a). According to chondrite normalized rare earth element (REE) diagrams Sun and McDonough (1989), the enrichment of light REE relatively to heavy REE with nearly flat HREE (Fig. 7 b) with a negative ($0.7-1$) Eu anomaly is observed for these rocks.

7. Discussion

7.1 Source of leucosome

Genetically, the leucosome portion of migmatite in the orogenic belt can either originate from the anatexis of metapelite or meta-mafic rocks in the high-grade metamorphic zone Hobson et al. (1998), Hinchey et al. (2006), Saki et al. (2012), Saki et al. (2020), and Yang et al. (2020). The leucosome portion released from the pelitic rocks is characterized by $K_2O/Na_2O > 1$ and A/CNK > 1 as compared to mafic-derived leucosomes, in addition to high corundum normative. The low K_2O/ Na_2O (< 0.06), A/CNK (< 1), and lack of corundum normative in the studied leucosome from BIC exclude the metapelite as a protolith for these migmatites. Moreover, the low ratios of Rb/Sr (< 0.1) combined with low Rb/Ba (< 0.07) in addition to high SiO_2 with low Rb/Zr (< 0.2) in the studied leucosome suggest consistency with mafic protoliths. Furthermore, the low TiO_2 content in the leucosome of BIC at a given SiO_2 value may support a partial melting process for its formation (Koepke et al., 2007).

Experimental petrology in the felsic melts with Tonalite-Trondhjemite- Granodiorite (TTG) will be produced for the partial melting on the lower crust with the mafic composition (amphibolite and gabbro). Furthermore, experimental works Rapp et al. (1991), Yaxley and Sobolev (2007), and Qian and Hermann (2013), demonstrated that melanosome mineral and type are related to ratios of partial melting, temperature, and pressure. For example, $10-40$ % partial melting ratios of the mafic rocks make a residue with the different paragenesis: plagioclase + amphibole ± garnet (amphibolite) at $0.8-1.5$ GPa and $1000-800$ ^{O}C; plagioclase + amphibole + garnet + clinopyroxene + orthopyroxene (garnet granulite) at 1.25 GPa and 900 ^{O}C; plagioclase + clinopyroxene + orthopyroxene ± amphibole (two-pyroxene granulite) at 1 GPa and 900 ^{O}C and $1-1.25$ GPa and 1,000 ^{O}C, garnet + clinopyroxene ± amphibole (garnet pyroxenite) at $1.35-1.5$ GPa and $900-1,000$ ^{O}C; clinopyroxene + orthopyroxene (pyroxenite) at 1.5 GPa and 1050 ^{O}C.

Based on the reported experimental paragenesis, a significant conclusion is drawn. Garnet is identified as a mineral that is sensitive to changes in pressure and temperature (P-T) conditions. As a result, it can serve as a valuable diagnostic indicator mineral. Specifically, it can aid in distinguishing between high P-T conditions (above 800 ^{O}C and beyond 1 GPa) and low P-T conditions (below 800 ^{O}C and under 1 GPa) during partial melting processes of mafic rocks. The absence of garnet within the residual amphi-

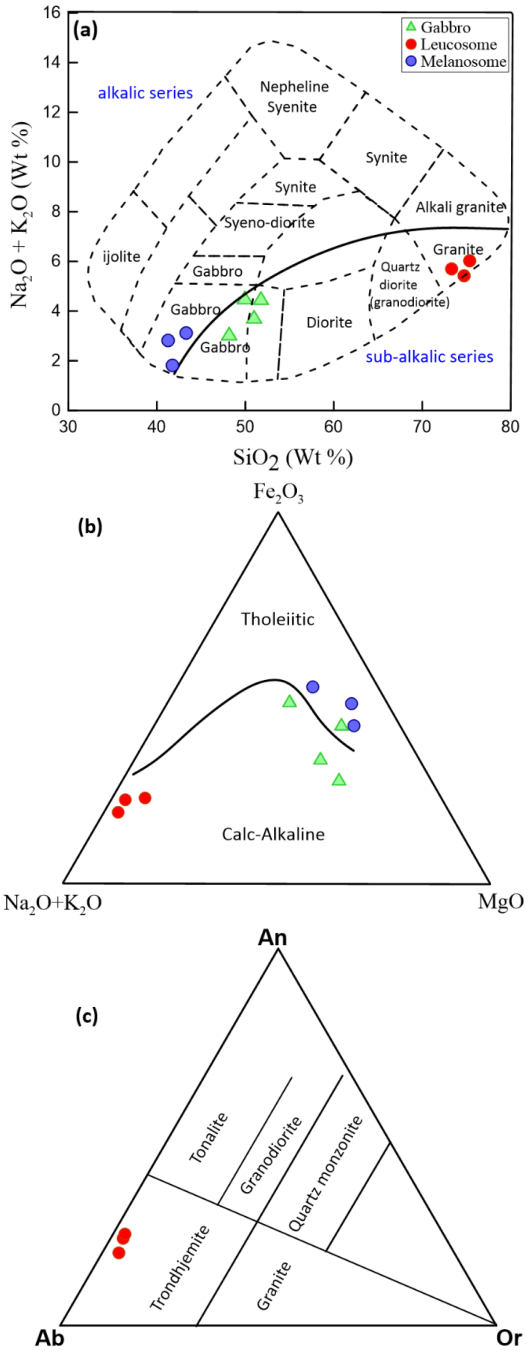

Figure 6. Chemical classification diagrams for the studied Qandol migmatites (Source, leucosome, and melanosome) (a) Total alkali versus SiO_2 (TAS) diagram (Cox et al., 1979) (b) AFM ternary diagram of (Irvine and Baragar, 1971). (c) Leucosome compositions plotted on the normative An-Ab-Or classification diagram (O'Conner, 1965).

bolitic melanosome in the Qandol area, as outlined in the petrography section, indicates low P-T conditions. This suggests that the anatexis (partial melting) of gabbroic rock likely occurred at relatively shallow depths. Furthermore, the presence of hornblende and biotite in most of the protolith samples (Fig. 5) suggests that an ample supply of water was available within the rock prior to the melting event. This presence of water-rich minerals is indicative of conditions conducive to partial melting processes.

The sandwiched of high-grade metamorphic rocks between the mantle peridotite in the east and Bulfat gabbroic in the west with highly sheared mylonitic structure and the metamorphic segregation layers may suggest that the partial melting has occurred in high temperatures (1000 ^{O}C), and low pressure (0.2 – 0.3 GPa) melting regimes based on the (Hobson et al., 2000). Here seems that the migmatization may occur due to the hydrous partial melting of mafic rocks, as in the following equation:

Ol + CPX + PL (Ca-Na rich) + H_2O → Residue (HBL + OPX + Pl (Ca-rich) + Hydrous TTG melt (Na-rich plagioclase) (Wolff et al., 2013).

7.2 Pressure and temperature (P-T) estimation

Barker and Arth (1976), introduced the concept that the Al_2O_3 content of tonalite-trondhjemite-granodiorite (TTG) compositions can be used as a barometer to infer the pressure conditions during the formation of TTG magmas. Rapp et al. (1991), through experimental investigations involving mafic rocks, established a relationship between Al_2O_3 content and pressure. Specifically, they observed a gradual increase in Al_2O_3 content with increasing pressure. In TTG magmas, Rapp et al. (1991), found that the Al_2O_3 content is typically < 15 wt.% at pressures around 0.8 GPa, but it exceeds 15 wt.% at pressures exceeding 1.6 GPa. The relatively low Al_2O_3 contents (an average of 14.5 wt.%) of the studied leucosome samples from BIC suggest that its magma was formed under relatively low-pressure conditions with the restite comprising amphibole, plagioclase, and orthopyroxene (Rapp et al., 1991). The restite comprising new plagioclase is coincident with the negative Eu and

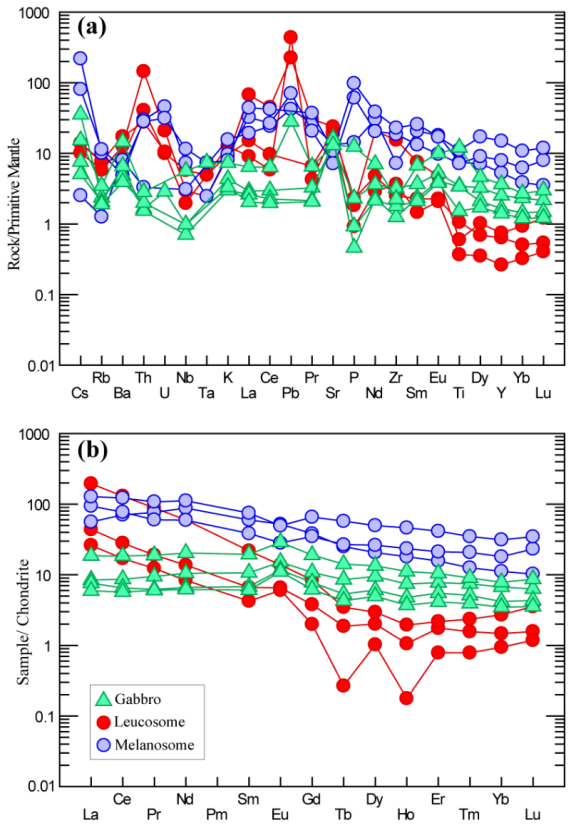

Figure 7. (a) Primitive mantle normalized trace element diagram (Sun and McDonough, 1989) (b) (Sun and McDonough, 1989) chondrite-normalized rare earth element diagram for the Qandol migmatites.

Sr anomalies shown in (Fig. 8). Moreover, all the leucosome samples form BIC plots in the low-pressure field on the An–Ab–Or diagram (Fig. 8); (Winter, 2001). Due to the absence of microprobe data for amphibole and plagioclase in the current stage of the study on the BIC, an alternative and reliable approach is taken for estimating the initial melt temperature. This estimation is based on zircon saturation thermometry (Watson and Harrison, 1983). The simulation formula of zircon solubility is as follows: TZr (^{O}C) = {12,900 [lnDZr (496,000/melt) + 0.85 M + 2,195]} − 273.15.

The calculated Zircon Saturation Temperature (TZr) for the leucosomes within the BIC falls within the range of 642 to 791 ^{O}C (Table 1). This range represents the initial temperature of the tonalite-trondhjemite-granodiorite (TTG) magma. The relatively low temperature value, being below 850 ^{O}C, indicates a scenario of low-degree partial melting (France et al., 2010). Furthermore, the high SiO_2 contents observed in the leucosome samples from the BIC provide further support for the notion of a low degree of partial melting. This is consistent with the inference that less than 10% of the source rock underwent melting (**Johannes2012**).

Furthermore, the estimation of the P-T condition of the granitic rock has been successfully manifested and validated based on the CIPW normative. The Ab–An–Or diagram for the studied leucosome suggests their crystallization condition at a temperature range of $670-700$ ^{O}C at a low pressure of ~ 0.1 GPa.

7.3 Pseudosection based on the GeoPS

In order to demonstrate the process of partial melting and the subsequent evolution of mineral assemblages in mafic rocks, we performed phase equilibrium modeling (pseudosection) using GeoPS software **Xiang2021<empty citation>**, version 3.2; data set ds62 in the system NCFMASHT (Na_2O-CaO-Fe_2O_3-MgO-Al_2O_3-SiO_2-H_2O-TiO_2).The selected solid-solution models are amphibole and augite Green et al. (2016), feldspars Hollan and Powell (2003), garnet, biotite, orthopyroxene, and melt White et al. (2014), ilmenite White et al. (2000), and spinal (White et al., 2002).

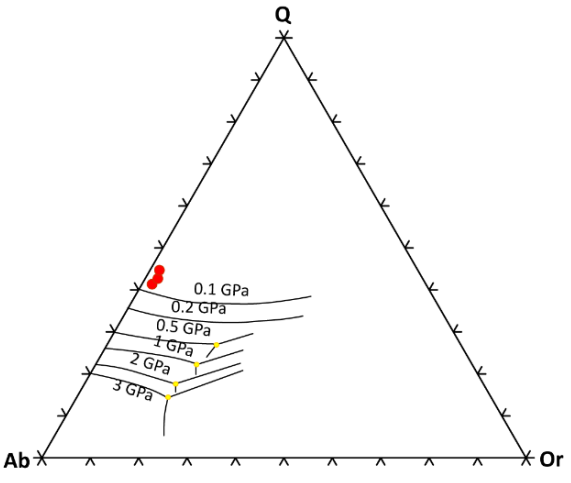

Figure 8. The Ab–Or–Q scheme with the ternary cotectic curves (Winter, 2001), which shows the leucosome parts plot in the low-pressure field with less than 0.1 GPa (Gigapascal).

K_2O is skipped in our phase modeling calculation because it occupies very little of the whole-rock composition.

In general, mafic rocks such as gabbro are investigated to melt under hydrous partial melting processes, and the existence of extra water causes a partial melting reaction to occur at lower temperatures (Lambert and Wyllie, 1972; Springer and Seck, 1997; Wolff et al., 2013). We add additional water (4 wt.%) for calculation (Fig. 9) to show the role of water in the reaction. Calculating the pseudosections at a temperature between 600 and 1000 ^{O}C and a pressure between 0.1 and 1 GPa (Fig. 9). The first melt appeared at 720 ^{O}C, while the appropriate mineral assemblage amphibole + clinopyroxene + Ilmenite + orthopyroxene + plagioclase + Melt + H_2O entrance at 790 ^{O}C − 920 ^{O}C and 0.1 to 0.4 GPa. Garnet appears within the melt as the pressure increases (up to 0.95 GPa). Hence, thermobarometer modeling proposes to show that gabbro partially melted at high temperatures and low pressure to form leucosomes in the Qandol area.

7.4 P-T-t for the migmatites

Zircon geochronology combined with Ar-Ar geochronology of various rock units of BIC and the calculated P–T path derived from single mineral (hornblende thermometry) and mineral phase equilibrium based on the bulk rock chemistry were used to distinguish two stages of magmatic rocks has been overprinted by the regional collisional tectonothermal events (Nutman et al., 2022). The 39 - 41 Ma ^{39}Ar - ^{40}Ar Aswad et al. (2016), older gabbroic and dioritic body ($634-698\pm50$ ^{O}C and 2.5 GPa), was cut by the younger 39.0 ± 0.5 Ma U-Pb zircon olivine gabbro intruded at $\sim 950-1050$ ^{O}C and $\sim 0.3-0.5$ GPa (Ali, 2017). The high-grade metamorphic rocks here have been considered contact metamorphism due to the injection of hot mafic magma into the Qandil formation (Karo et al., 2018). Furthermore, Karo et al. (2018) considered peak metamorphism conditions in the range of $605-671$ ^{O}C and $0.28-0.35$ GPa at 34.78 Ma. The trondhjemite dikes that have cut the younger olivine gabbro of the BIC show 48 Ma U-Pb ages (Nutman et al., 2022). Also, they suggested the partial melting of the mafic rocks for the sources of TTG rocks here. Moreover, the host igneous intrusions should be older than the trondhjemite dikes that have cut them.

7.5 Tectonic significant of migmatite in Zagros orogenic belt

Migmatites formed from mafic rocks are uncommon and are typically constrained to specific geological settings. These settings include: (i) the core of the orogenic belts and (ii) the roots of a volcanic edifice (Vanderhaeghe, 2009).

(i) Migmatite in orogenic belts

This particular type of migmatite could correspond to three consecutive stages in the thermal-mechanical evolution of a hypothetical orogenic belt. These stages are outlined as follows: (a) The initial phase is characterized by the formation of an orogenic wedge, which occurs during the early stage (t1). (b) Subsequent to the orogenic wedge formation, the orogenic belt experiences the development of a continental plateau, representing the middle stage (t2). (c) The final phase involves the gravitational collapse of the oro-

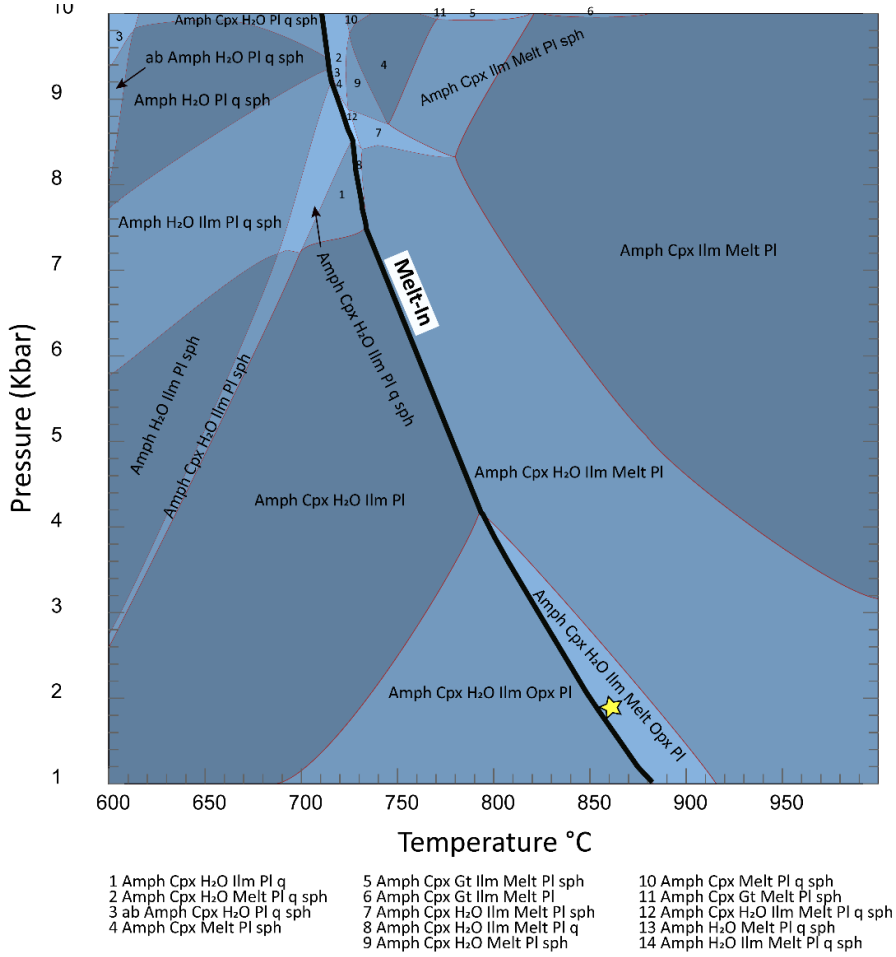

Figure 9. Computed Phase diagram for the Qandol migmatite (sample QBA-20) with extra water (4%) based on bulk composition (Table 1). The black line represents the first melt in the system.

genic belt, constituting the late stage (t3). In the context of this orogenic belt, mafic migmatites of lower crustal origin emerge and are pushed towards the periphery of the continental plateau. This movement occurs through processes such as lateral flow and intrusion (Vanderhaeghe, 2009).

In the orogenic belts, mantle heat advection associated with plate motion and associated heat conduction are the main sources of temperature (Vanderhaeghe, 2009). The hot collision of the Arabian plate passive continental margin with the southern active continental margin of Eurasia, represented by SaSZ, is an ongoing process that started in the Eocene and is nowadays reflected by the Zagros orogenic belt. Since the collision, Arabia has continued to converge and penetrate north-northeast into Eurasia, resulting in the doubled crust beneath the Zagros and SaSZ fields (Talebi et al., 2020). Following the Arabia–Iranian collision, crustal thickening, and shortening (by folding and thrusting) along the northern margin of Arabia may result in increased pressure and temperatures. During the early stage of the Zagros orogenic wedge, increasing temperature and decreasing pressure events resulted in decompression melting within the upper part of the middle crust (metapelite) of the Zagros. One of the most notable outcomes of the intense collision that shaped the Zagros Mountains was the creation of leucogranites through the partial melting of rocks within a widespread zone of migmatites found in the middle crust around 40 million years ago. This process is potentially exemplified by the Baneh S-type granite Azizi et al. (2019), covering an area of approximately 100 square kilometers, situated at the central region of the Zagros orogenic belts. Within the Sanandaj-Sirjan Zone of the Zagros orogenic belt in Iran, remnants of Jurassic pelitic and mafic migmatites have been observed. The origin of the Jurassic mafic migmatite within this zone is attributed to the upwelling of magma from the asthenosphere within the magmatic arc, rather than being a direct result of the collision between the Arabian and Iranian plates (Saki et al., 2020).

(ii) Roots of a volcanic edifice migmatite

The magmatic evolution of the mature arcs spans around 20 – 30 Ma (Stern, 2002). Continuing successive arc magmatism causes anatexis of the lower mafic crust, along with the transformation of the old mafic crustal base component into the mantle through the Moho, finally creating a mature arc crust. The distilling of felsic magmas from mantle-derived juvenile crust via anatexis of mafic rock may produce a mafic migmatite at the base of a mature volcanic arc through a limited anatexis process. Thus, the physiographical nature of the Bulfat igneous metamorphic complex, as represented by the domal shape of the intrusion, in addition to complete sequences of mature arc combined with the age of migmatite leucosome suggests that the migmatite

of Bulfat represents the root of the mature magmatic arc rather than the collision-related migmatite. The development of the highly sheared structures in the high-grade metamorphic rocks, which we considered as migmatite in this research, and also the differential of the mafic and felsic members as separate bands, which occurred in the highly sheared zone, implies that the metamorphism occurred in a high-temperature sheard zone not in contact metamorphism around a mafic body. In addition, there is some misinterpretation of Bulfat gabbro, our field observation shows the BIC includes volcanic members, with some pelagic sediments, and metagabbroic members with Late Cretaceous ages. Probably they are representing the dismembered parts of the Zagros ophiolite with Late Cretaceous ages. Therefore, it cannot make a high-grade metamorphism in the Eocene here. In addition, only the migmatites were observed at the junction of the BIC in the west and the mantle peridotite in the east on the Iranian side in the Qandol area. Furthermore, new radiometric ages have shown that trondhjemitic rocks, which are the results of mafic partial melting were generated 48 Ma ago (Nutman et al., 2022).

Therefore, we suggest two main scenarios for the genesis of these rocks. First, these rocks may be generated from the anatexis of gabbroic root zone of mature intraoceanic arc, making a locally highly metamorphic rock in the area. The second scenario is the subduction of a hot oceanic crust, and probably it can make a high-grade zone in a shallow depth. Actually, we could not clearly find the reverse grade of the metamorphism, but we cannot ignore this proposal completely, and now the question remains whether the rocks are the sole metamorphic rock underlying ophiolite or not. This proposal is much supported by the hydration of the ultramafic rocks, which are highly deformed and were changed to serpentinite, and probably may infer that the overridden plate was cold during the thrusting. Finally, we believe more work on these rocks is more obvious and concealed of the Zagros geology. It may be possible to find some more outcrops for these rocks on the border of Iran and Iraq, but unfortunately, this area has many restrictions for the geology study.

8. Conclusions

Qandol migmatite in the BIC consists of stomatic and fold structures. These migmatites are just visible at the intersection of the metagabbro component of BIC in the west and the mantle peridotite in the east. Field observation and thermodynamic modeling of the migmatite in this area may suggest that the migmatization process of the mafic rocks to produce leucosome and melanosome associations were occured by hydros partial melting at low pressure ($0.1 - 0.4$ GPa) and high temperature ($790\ ^{o}C - 920\ ^{o}C$) at the root of the volcanic edifice in the Qaladiza area. The results of the present study show that these rocks may also been formed by subduction of the hot Neotethys oceanic crust beneath the SaSZ (western Iran) during the Late Cretaceous-Paleocene before collision of the Arabian and Iran Plates in the Eocene. The mineralogy and calculated P-T condition of the metamorphism which infer the high T and Low P metamorphism facies. We suggest that the migmatites locally were formed by dragging of the mafic parts at the initiation of hot oceanic subduction. Finlay they obductued due to continuity of the oceanic subduction and or during the collision. So, the ages of emplacement of these rocks is a bit ambiguous and need some dating.

Acknowledgments

This paper is part of the Ph.D. thesis of the first author. We are grateful to N. Daneshavar for unlimited support. The revised version benefited from the two anonymous reviewers and chief editor R. Dabiri.

Authors contributions

All the authors have participated sufficiently in the intellectual content, conception and design of this work or the analysis and interpretation of the data (when applicable), as well as the writing of the manuscript.

Availability of data and materials

The data that support the findings of this study are available from the corresponding author, upon reasonable request.

Conflict of interests

The authors declare that they have no known competing financial interests or personal relationships that could have appeared to influence the work reported in this paper.

References

Ali S. A. (2017) 39Ma U-Pb zircon age for the Shaki-Rash gabbro in the Bulfat igneous complex, Kurdistan region, Iraqi Zagros Suture zone: rifting of an Intra-Neotethys Cenozoic arc. *Ofioliti* 42:69–80. DOI: https://doi.org/10.4454/ofioliti.v42i2.485.

Ashworth J., McLellan E. (1985) *Textures, in: Ashworth, J.R. (eds) Migmatites. Springer,* 180–203. DOI: https://doi.org/10.1007/978-1-4613-2347-1“˙5.

Aswad K. J., Ali S. A., Sheraefy R. M., Nutman A., Buckman S., Jones B. G., Jourdan F. (2016) $^{40}Ar/^{39}Ar$ hornblende and biotite geochronology of the Bulfat Igneous Complex, Zagros Suture Zone, NE Iraq: New insights on complexities of Paleogene arc magmatism during closure of the Neotethys Ocean. *Lithos* 266:406–413. DOI: https://doi.org/10.1016/j.lithos.2016.10.013.

Aswad K. J., Aziz N. R., Koyi H. (2011) Cr-spinel compositions in serpentinites and their implications for the petrotectonic history of the Zagros Suture Zone, Kurdistan Region, Iraq. *Geological magazine* 148:802–818. DOI: https://doi.org/10.1017/S0016756811000422.

Aziz N. R., Aswad K. J., Koyi H. (2011) Contrasting settings of serpentinite bodies in the northwestern Zagros Suture Zone, Kurdistan Region, Iraq. *Geological Magazine* 148:819–837. DOI: https://doi.org/10.1017/S0016756811000409.

Azizi H., Hadad S., Stern R. J., Asahara Y. (2019) Age, geochemistry, and emplacement of the∼ 40-Ma Baneh granite–appinite complex in a transpressional tectonic regime, Zagros suture zone, northwest Iran. *International Geology Review* 61:195–223. DOI: https://doi.org/10.1080/00206814.2017.1422394.

Barker F., Arth J. (1976) Generation of trondhjemitic-tonalitic liquids and Archean bimodal trondhjemite-basalt suites. *Geology* 4:596–600. DOI: https://doi.org/10.1130/0091-7613(1976)4“%3C596:GOTLAA“%3E2.0.CO;2.

Brown M., Averkin Y., McLellan E., Sawyer E. (1995) Melt segregation in migmatites. *Journal of Geophysical Research: Solid Earth* 100:15655–15679. DOI: https://doi.org/10.1029/95JB00517.

Buda G. (1993) Igneous petrology of the Bulfat area (north-east Iraqi Zagros thrust zone). *Acta Mineralogica Petrographica* 34:21–39.

Cox K., Bell J., Pankhurst R. (1979) The interpretation of igneous rocks. *George Allen,* DOI: https://doi.org/10.1007/978-94-017-3373-1.

Elias E., Al-Jubory Z., Aqrawi A. (2022) Metamorphic evolution of the bulfat belt (NE-Iraq): Evidence from $^{40}Ar/^{39}Ar$ age spectrum measurements. *The Iraqi Geological Journal,* 1–11. DOI: https://doi.org/10.46717/igj.55.1E.1Ms-2022-05-17.

France L., Koepke J., Ildefonse B., Cichy S., Deschamps F. (2010) Hydrous partial melting in the sheeted dike complex at fast spreading ridges: experimental and natural observations. *Contributions to Mineralogy and Petrology* 160:683–704. DOI: https://doi.org/10.1007/s00410-010-0502-6.

Green E., White R., Diener J., Powell R., Holland T., Palin R. (2016) Activity–composition relations for the calculation of partial melting equilibria in metabasic rocks. *Journal of metamorphic Geology* 34:845–869. DOI: https://doi.org/10.1111/jmg.12211.

Gurbuz A., Saein A. (2019) Tectonic geomorphology of the Zagros orogen. *in Developments in Structural Geology and Tectonics (Elsevier),* 131–144. DOI: https://doi.org/10.1016/B978-0-12-815048-1.00008-1.

Hinchey A., Carr S., McNeill P., Rayner N. (2006) Paleocene–Eocene high-grade metamorphism, anatexis, and deformation in the Thor–Odin dome, Monashee complex, southeastern British Columbia. *Canadian Journal of Earth Sciences* 43:1341–1365. DOI: https://doi.org/10.1139/e06-028.

Hobson A., Bussy F., Hernande J. (2000) Migmatitic gabbros from a shallow-level metamorphic contact aureole, Fuerteventura Basal Complex, Canary Islands: role of deformation in melt segregation, in Physics and chemistry of partially molten rocks. *Springer* 11:209–227. DOI: https://doi.org/10.1007/978-94-011-4016-4“¨7.

Hobson A., Bussy F., Hernandez J. (1998) Shallow-level migmatization of gabbrosin a metamorphic contact aureole, fuerteventura basal complex, canary islands. *Journal of Petrology* 39:1025–1037. DOI: https://doi.org/10.1093/petroj/39.5.1025.

Hollan T., Powell R. (2003) Activity–composition relations for phases in petrological calculations: an asymmetric multicomponent formulation. *Contributions to Mineralogy and Petrology* 145:492–501. DOI: https://doi.org/10.1007/s00410-003-0464-z.

Irvine T., Baragar W. (1971) A guide to the chemical classification of the common volcanic rocks. *Canadian journal of earth sciences* 8:523–548. DOI: https://doi.org/10.1139/e71-055.

Jassim S., Goff J. (2006) Geology of Iraq. Dolin, sro, distributed by Geological Society of London.

Karo N., Oberhansli R., Aqrawi A., Elias E., Aswad K. J., Sudo M. (2018) New $^{40}Ar/^{39}Ar$ age constraints on cooling and unroofing history of the metamorphic host rocks (and igneous intrusion associates) from the Bulfat Complex (Bulfat area), NE-Iraq. *Arabian Journal of Geosciences* 11:1–11. DOI: https://doi.org/10.1007/s12517-018-3571-x.

Koepke J., Berndt J., Feig S., Holtz F. (2007) The formation of SiO_2-rich melts within the deep oceanic crust by hydrous partial melting of gabbros. *Contributions to Mineralogy and Petrology* 153:67–84. DOI: https://doi.org/10.1007/s00410-006-0135-y.

Lambert I., Wyllie P. (1972) Melting of gabbro (quartz eclogite) with excess water to 35 kilobars, with geological applications. *The Journal of Geology* 80:693–708. DOI: https://doi.org/10.1086/627795.

Le Garzic E., Verges J., Sapin F., Saura E., Meresse F., Ringenbach J. (2019) Evolution of the NW Zagros Fold-and-Thrust Belt in Kurdistan Region of Iraq from balanced and restored crustal-scale sections and forward modeling. *Journal of Structural Geology* 124:51–69. DOI: https://doi.org/10.1016/j.jsg.2019.04.006.

Maxeiner R., Ashton K., Card C., Morelli R., Knox B. (2017) A field guide to naming migmatites and their textures, with Saskatchewan examples. *Summary of Investigations* 2:2017–4.

Mohammad Y., Abdulla K., Azizi H. (2023) Late cretaceous-paleocene arc and back-arc system in the neotethys ocean, Zagros suture zone. *Minerals* 13:1367. DOI: https://doi.org/10.3390/min13111367.

Mohammad Y., Cornell D., Qaradaghi J., Mohammad F. (2014) Geochemistry and Ar–Ar muscovite ages of the Daraban Leucogranite, Mawat Ophiolite, northeastern Iraq: implications for Arabia–Eurasia continental collision. *Journal of Asian Earth Sciences* 86:151–165. DOI: https://doi.org/10.1016/j.jseaes.2013.09.029.

Mohammad Y., Kareem H., Anma R. (2016) The Kuradawe granitic pegmatite from the Mawat ophiolite, Northeastern Iraq: Anatomy, mineralogy, geochemistry, and petrogenesis. *The Canadian Mineralogist* 54:989–1019. DOI: https://doi.org/10.3749/canmin.1600028.

Nutman A., Ali S. A., Mohammad Y., Jones B., Zhang Q. (2022) The early Eocene (48 Ma) Qaladeza trondhjemite formed by wet partial remelting of mafic crust in the arc-related Bulfat Igneous Complex (Kurdistan, Iraq): constraints on the timing of Neotethys closure. *Arabian Journal of Geosciences* 15:1–11. DOI: https://doi.org/10.1007/s12517-022-09975-7.

O'Conner J. (1965) A classification of quartz-rich igneous rocks based on feldspar ratios, US Geological Survey. *Professional Papers* 525B:B79–B84.

Pawley M., Preiss W., Dutch R., Reid A. (2013) A User's Guide to Migmatites. Department for Manufacturing, Innovation, Trade. *Resources and Energy*

Qian Q., Hermann J. (2013) Partial melting of lower crust at 10–15 kbar: constraints on adakite and TTG formation. *Contributions to Mineralogy and Petrology* 165:1195–1224. DOI: https://doi.org/10.1007/s00410-013-0854-9.

Rapp R., Watson E., Miller C. (1991) Partial melting of amphibolite/eclogite and the origin of Archean trondhjemites and tonalites. *Precambrian Research* 51:1–25. DOI: https://doi.org/10.1016/0301-9268(91)90092-O.

Saki A., Miri M., Oberhansli R. (2020) High temperature–low pressure metamorphism during subduction of Neo-Tethys beneath the Iranian plate: evidence for mafic migmatite formation in the Alvand complex (western Iran). *Mineralogy and Petrology* 114:539–557. DOI: https://doi.org/10.1007/s00710-020-00721-z.

Saki A., Moazzen M., Baharifar A. (2012) Migmatite microstructures and partial melting of Hamadan metapelitic rocks, Alvand contact aureole, western Iran. *International geology review* 5:1229–1240. DOI: https://doi.org/10.1080/00206814.2011.636639.

Sawyer E. (2010) Migmatites formed by water-fluxed partial melting of a leucogranodiorite protolith: Microstructures in the residual rocks and source of the fluid. *Lithos* 116:273–286. DOI: https://doi.org/10.1016/j.lithos.2009.07.003.

Sawyer E., Brown M. (2008) Working with migmatites: Mineralogical association of Canada. *Short Course Series* 38:158.

Springer W., Seck H. (1997) Partial fusion of basic granulites at 5 to 15 kbar: implications for the origin of TTG magmas. *Contributions to Mineralogy and Petrology* 127:30–45. DOI: https://doi.org/10.1007/s004100050263.

Stern R. (2002) Subduction zones. *Reviews of geophysics* 40:3–1. DOI: https://doi.org/10.1029/2001RG000108.

Sun S. S., McDonough W. F. (1989) Chemical and isotopic systematics of oceanic basalts: implications for mantle composition and processes, Geological Society. *London, Special Publications* 42:313–345. DOI: https://doi.org/10.1144/GSL.SP.1989.042.01.19.

Talebi A., Koulakov I., Moradi A., Rahimi H., Gerya T. (2020) Ongoing formation of felsic lower crustal channel by relamination in Zagros collision zone revealed from regional tomography. *Scientific reports* 10:1–7. DOI: https://doi.org/10.1038/s41598-020-64946-w.

Vanderhaeghe O. (2009) Migmatites, granites and orogeny: Flow modes of partially-molten rocks and magmas associated with melt/solid segregation in orogenic belts. *Tectonophysics* 477:119–134. DOI: https://doi.org/10.1016/j.tecto.2009.06.021.

Watson E. B., Harrison T. M. (1983) Zircon saturation revisited: temperature and composition effects in a variety of crustal magma types. *Earth and planetary science letters* 64:295–304. DOI: https://doi.org/10.1016/0012-821X(83)90211-X.

Weinberg R. F., Mark G. (2008) Magma migration, folding, and disaggregation of migmatites in the Karakoram Shear Zone, Ladakh, NW India. *Geological Society of America Bulletin* 120:994–1009. DOI: https://doi.org/10.1130/B26227.1.

White R., Powell R., Clarke G. (2002) The interpretation of reaction textures in Fe-rich metapelitic granulites of the Musgrave Block, central Australia: constraints from mineral equilibria calculations in the system K_2O–FeO–MgO–Al_2O_3–SiO_2–H_2O–TiO_2–Fe_2O_3. *Journal of metamorphic Geology* 20:41–55. DOI: https://doi.org/10.1046/j.0263-4929.2001.00349.x.

White R., Powell R., Holland T., Johnson T., Green E. (2014) New mineral activity–composition relations for thermodynamic calculations in metapelitic systems. *Journal of Metamorphic Geology* 32:261–286. DOI: https://doi.org/10.1111/jmg.12071.

White R., Powell R., Holland T., Worley B. (2000) The effect of TiO_2 and Fe_2O_3 on metapelitic assemblages at greenschist and amphibolite facies conditions: mineral equilibria calculations in the system K_2O-FeO-MgO-Al_2O_3-SiO_2-H_2O-TiO_2-Fe_2O_3. *Journal of Metamorphic Geology* 18:497–511. DOI: https://doi.org/10.1046/j.1525-1314.2000.00269.x.

Whitney D. L., Evans B. W. (2010) Abbreviations for names of rock-forming minerals. *American mineralogist* 95:185–187. DOI: https://doi.org/10.2138/am.2010.3371.

Winter J. (2001) An introduction to Igneous and Metamorphic Petrology.An introduction to Igneous and Metamorphic Petrology

Wolff P. E., Koepke J., Feig S. T. (2013) The reaction mechanism of fluid-induced partial melting of gabbro in the oceanic crust. *European Journal of Mineralogy* 25:279–298. DOI: https://doi.org/10.1127/0935-1221/2013/0025-2314.

Xiang H., Connolly J. A. (2022) GeoPS: An interactive visual computing tool for thermodynamic modelling of phase equilibria. *Journal of Metamorphic Geology* 40:243–255. DOI: https://doi.org/10.1111/jmg.12626.

Yang Y., Liu YC., Li Y., Groppo C., Rolfo F. (2020) Zircon U-Pb dating and petrogenesis of multiple episodes of anatexis in the north dabie complex zone, central China. *Minerals* 10:618. DOI: https://doi.org/10.3390/min10070618.

Yaxley G., Sobolev A. V. (2007) High-pressure partial melting of gabbro and its role in the Hawaiian magma source. *Contributions to Mineralogy and Petrology* 154:371–383. DOI: https://doi.org/10.1007/s00410-007-0198-4.